Journal of Photochemistry and Photobiology A: Chemistry 199 (2008) 274–281

Contents lists available at ScienceDirect

Journal of Photochemistry and Photobiology A: Chemistry

journal homepage: www.elsevier.com/locate/jphotochem

Excited state processes of nitrobenzaldehydes probed by ultrafast fluorescence and absorption spectroscopy

B. Heinz, T. Schmierer, S. Laimgruber, P. Gilch*

Fakultät für Physik, Ludwig-Maximilians-Universität, Oettingenstr. 67, D-80538 München, Germany

ARTICLE INFO

Article history:
Received 8 April 2008
Received in revised form 21 May 2008
Accepted 2 June 2008
Available online 24 June 2008

Keywords:
Photochemistry
Femtosecond spectroscopy
Fluorescence
Absorption
Nitrobenzaldehyde
Hydrogen transfer
Intersystem crossing

ABSTRACT

We have investigated the isomers *ortho*-, *meta*-, and *para*-nitro-benzaldehyde (NBA) by means of ultrafast emission and absorption spectroscopy. The fluorescence dynamics of all three molecules are very similar and feature bi-phasic emission decays with time constants of <100 fs and ~ 1 ps. The first process goes along with a strong loss of oscillator strength, which we assume is the result of a non-radiative $^1\pi\pi^* \rightarrow {}^1n\pi^*$ transition. These commonalities are contrasted by qualitatively different transient absorption signatures: For the photo-reactive isomer *o*-NBA, signatures of a ketene intermediate in the electronic ground state are observed. Its formation time matches the slower component of the emission decay. The ketene afterwards experiences pronounced cooling dynamics on the picosecond timescale followed by its decay in the nanosecond regime. For the non-reactive isomers *m*- and *p*-NBA, time constants with values similar to the ones derived from the emission experiment are found in the absorption experiment. In addition, at later delay times, a distinct spectral signature is observed for both isomers which decays within ~ 1 ns and is assigned to a triplet state. This triplet decay is preceded by a process on the 10 ps timescale which we tentatively assign to a transition within the triplet manifold.

1. Introduction

Nitroarenes find widespread application in (industrial) synthetic chemistry [1]. Large scale production relies on the thermal chemistry of these compounds, but highly specialized applications make use of their photochemistry. In these applications, nitroarene residues serve as photolabile protecting groups [2–4]. While synthesizing a target molecule photolability can add another "dimension" in an orthogonal protection strategy [5]. It further allows for temporal and spatial control of chemical reactivity—properties exploited in DNA chip synthesis [6] and caged compound experiments [7,8].

These applications profit from knowledge on the fundamental photochemical and photophysical properties of these compounds. The knowledge should of course include information on their fluorescence properties since they map out the behavior of the primarily excited states. Yet, nitroarenes are often termed "non-fluorescent" [9] and so data on their fluorescence and particularly its time dependence are scare. Recently, Peon and co-workers have reported on the fluorescence decay of some polycyclic nitroarenes [9]. They have observed bi-phasic emission decays with fast time constants as short as ~ 50 fs and longer lived components on the picosecond timescale. For these molecules, intersystem crossing to a triplet state is believed to be the major deactivation channel of the excited singlet state which has very recently been supported by means of a theoretical investigation [10]. Participation of triplet states in the photochemistry and photophysics of nitroarenes is considered rather general [11–13]. Contrary to other aromatics, the triplet states of several nitroarenes have been shown to be short-lived (~ 1 ns) [12,13]. However, for nitroperylene – a polycyclic nitroarene larger than the ones studied by Peon and co-workers – experiments pointed to rapid internal conversion instead of intersystem crossing to hold responsible for the depletion of the excited singlet state [14].

To our knowledge no time-resolved fluorescence experiments on a nitrobenzene derivative have been reported so far. Such experiments are particularly important in the context of photolabile protection since many of the protecting groups used there are derived from nitrobenzene [2,3]. In this study, we present time dependent fluorescence and absorption spectra of the *ortho*-, *meta*-, and *para*-isomers of nitrobenzaldehyde (*o*-, *m*-, *p*-NBA). This enables us to compare a photo-reactive nitrobenzene derivative (*o*-NBA) with non-reactive ones (*m*-NBA, *p*-NBA). *o*-NBA photo-transforms into *ortho*-nitrosobenzoic acid (Scheme 1) [15], whereas *m*- and *p*-NBA have been shown to be photo-inert in most organic solvents [15–17]. The photoreaction of *o*-NBA is known

* Corresponding author. Tel.: +49 89 2180 9243; fax: +49 89 2180 9202.
E-mail address: Peter.Gilch@physik.uni-muenchen.de (P. Gilch).

1010-6030/$ – see front matter © 2008 Elsevier B.V. All rights reserved.
doi:10.1016/j.jphotochem.2008.06.011

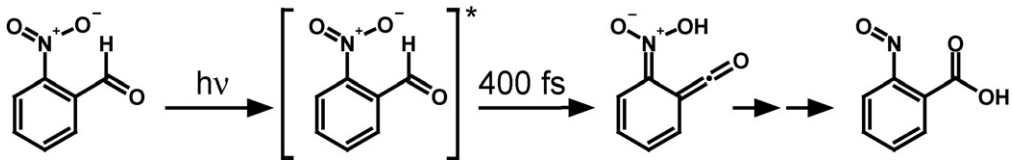

Scheme 1. Structures involved during the light-induced transformation of *o*-NBA to *o*-nitrosobenzoic acid.

for more than a century and its mechanism has been addressed by time-resolved studies with nano- and picosecond time resolution [18,19]. By means of femtosecond IR spectroscopy, we have recently shown that the first ground state intermediate of this reaction forms in 400 fs [20]. This intermediate adopts a ketene structure which results from an intramolecular hydrogen transfer. This fundamental chemical reaction step is considered canonical for all nitroarene based protecting groups [3,21]. Here, we will interconnect the formation of the ketene with the fluorescence decay. We will further present surprising commonalities in the fluorescence behavior of reactive and non-reactive isomers as well as distinct differences in the transient absorption signatures.

2. Experimental

The femtosecond fluorescence data were recorded using an optical Kerr-shutter which is described in detail in ref. [22]. In brief, a portion of the output of a 1 kHz laser/amplifier system (Clark CPA2001) was used to drive a non-collinear optical parametrical amplifier (NOPA) and an optical parametric amplifier (OPA). The NOPA generates pulses at 540 nm, which were frequency doubled to eventually yield the excitation light at 270 nm with a pulse energy of ~ 500 nJ/pulse. At the sample location this beam was focussed down to a diameter of ~ 150 μm. The OPA delivered the gate pulses at 1100 nm with 28 μJ/pulse. The Kerr-medium, a fused silica plate with a thickness of 0.32 mm, is placed between two wire grid polarizers (Moxtek, PLL04 fused silica substrate). Fluorescence was collected employing solely reflective aluminium coated optics and detected after spectral dispersion using a liquid nitrogen cooled CCD array. An appropriate filter (KG5) was used to reject strayed gate light. At each delay position data were accumulated for 5 s and the results of 30–50 scans of the time delay were averaged. To determine the time resolution of the experiment, the autocorrelation widths (FWHM) of pump (65 fs) and gate (40 fs) pulses were recorded. Based on these pulse durations, the width of the experimental response function should be around 80 fs. Since the fluorescence light and the gate pulse propagate through the Kerr-medium with different group velocities, the effective response time will be higher. A calculation based on the dispersion properties can account for that and yields an instrumental response time of 100–110 fs. The experimental dependencies of time zero $t_0(\lambda)$ due to group velocity dispersion as well as the spectral sensitivity of the gating process have been taken into account. Further, the effect of re-absorption by the sample as well as the spectral sensitivity of the setup have been thoroughly corrected for. In the latter procedure, a black-body radiator served as a reference for wavelengths larger than 460 nm [22]. For smaller wavelengths, we resorted to the well characterized fluorescence of 1-methyl naphthalene [23] as a reference. As the absorption of the sample rises and the spectral sensitivity drops with decreasing wavelength a reliable correction is only possible for wavelengths >320 nm. The steady state fluorescence spectrum was obtained using the Kerr-gate setup with the gate pulse blocked and the second polarizer removed for better transmission.

In the transient absorption experiments, the frequency tripled fundamental of a femtosecond laser/amplifier system (Clark CPA 2001) served as pump light (258 nm, 800 nJ/pulse, ~ 100 μm diameter at the sample location). White light pulses with magic angle polarization with respect to the pump pulse were used as probe light and detected with a 512-channel diode array read out at 1 kHz [24]. The data presented is an average of six delay scans, each with an acquisition time of 4 s at every delay position. To determine the time resolution of 200 fs (FWHM) and correct for dependencies of time zero $t_0(\lambda)$ due to group velocity dispersion the Kerr-effect induced by the pump pulse in a solvent jet was used to gate the probe light.

In all experiments, the sample solutions were flown through the excitation region using a wire-guided jet [24,25]. The thickness of the jet was ~ 250 μm and the flow rate ensured a sample exchange in between consecutive laser shots. The absorption of the respective sample was adjusted to ~ 1.5 OD at the excitation wavelength. Acetonitrile (Sigma–Aldrich, Chromasolv) served as solvent in all measurements performed. The NBA isomers as well as thymidine were purchased and used as received (*o*-NBA Merck >99%, *m*-NBA Aldrich 99%, *p*-NBA Aldrich 98%, thymidine Fluka >99%).

The time-resolved data were analyzed using a global fitting procedure. Here, it is assumed that the signal $S(\lambda, t)$ can be modeled using a sum of exponential decays convoluted with a Gaussian instrumental response function IRF:

$$S(\lambda, t) = \mathrm{IRF} \otimes \left(\sum_{i=1}^{n} A_i(\lambda) \mathrm{e}^{-(t-t_0)/\tau_i} \right) \quad \text{with} \quad t - t_0 \geq 0$$

In this representation, $A_i(\lambda)$ is the amplitude associated with the time constant τ_i at the wavelength λ. The FWHM values of the instrumental response functions IRF of the respective experiment have been determined as stated above.

3. Results

3.1. Fluorescence experiments

The absorption spectrum of *o*-NBA features several rather broad transition bands which strongly overlap with each other (Fig. 1). The weak red wing of the absorption extends to almost 400 nm. In the emission experiments, the excitation wavelength was tuned to 270 nm for the sake of comparison with earlier work [20]. When excited with 270 nm femtosecond pulses all solvents tested emit an appreciable background emission. This emission is dependent on the batch and bottle of the respective solvent used and often surmounts that of *o*-NBA. Acetonitrile features the lowest background emission and was thus chosen for the present study. We have inspected the concentration and intensity dependencies of acetonitrile solutions of *o*-NBA assuring that the genuine emission from *o*-NBA has been observed. Its fluorescence extends from below 320 nm to beyond 600 nm (Fig. 1) and features a maximum around 355 nm. The maximum of the fluorescence spectrum is higher in energy than the lowest absorption band of *o*-NBA (see spectral deconvolution in ref. [26]). This clearly shows that emission from a higher excited state is observed.

The quantum yield of this emission can be determined by comparison with the fluorescence of thymidine (inset in Fig. 1). The

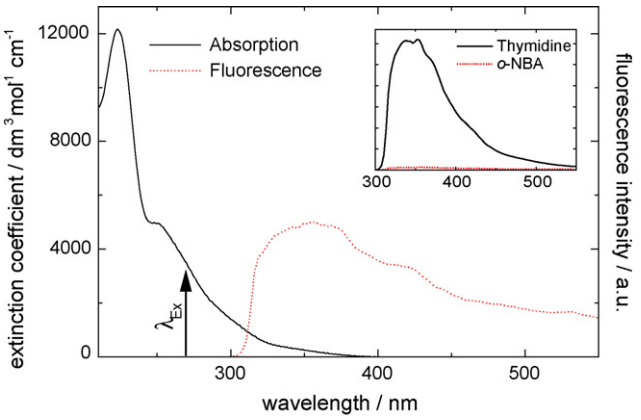

Fig. 1. UV–vis spectrum (solid line) and steady state fluorescence spectrum (dotted) of *o*-NBA after excitation at 270 nm. The modulation on top of the fluorescence signal is due to the imperfectness of the spectral correction and residual strayed light within the setup. The inset compares the fluorescence intensities of thymidine (solid) and *o*-NBA (dotted).

integrated emission spectra of *o*-NBA and thymidine exhibit a ratio of ∼ 1/30. As the integration did not cover the complete spectrum of *o*-NBA this ratio represents a lower limit for the relative fluorescence intensity of *o*-NBA. The fluorescence quantum yield of thymidine in aqueous solution amounts to $\sim 1 \times 10^{-4}$ [27,28]. Assuming a similar value to hold for thymidine in acetonitrile, the fluorescence quantum yield of *o*-NBA is as low as $\sim 4 \times 10^{-6}$. This extremely low value already indicates the very rapid depopulation of the emissive excited state(s). The fluorescence quantum yield ϕ_{fl} is given by the ratio of the fluorescence lifetime τ_{fl} and the radiative lifetime τ_{rad}

$$\phi_{fl} = \frac{\tau_{fl}}{\tau_{rad}}.$$

For the yield of *o*-NBA, ϕ_{fl}^{NBA} in relation to that of thymidine ϕ_{fl}^{T} this implies

$$\frac{\phi_{fl}^{NBA}}{\phi_{fl}^{T}} = \frac{\tau_{fl}^{NBA}}{\tau_{fl}^{T}} \cdot \frac{\tau_{rad}^{T}}{\tau_{rad}^{NBA}} \approx \frac{\tau_{fl}^{NBA}}{\tau_{fl}^{T}} \cdot \frac{\epsilon_{NBA}}{\epsilon_{T}}.$$

The second approximate equality holds since the radiative rate $1/\tau_{rad}$ is proportional to the extinction coefficient ϵ [29], provided that the absorption bands have similar widths. With our Kerr-gate setup, we have measured the transient fluorescence of thymidine and determined τ_{fl}^{T} in acetonitrile to be 0.32 ps. This value is in line with the value of 0.47 ps found for thymidine in water [28]. Based on the extinction coefficients, $\epsilon_{NBA} = 4000\,M^{-1}\,cm^{-1}$ and $\epsilon_{T} = 10,500\,M^{-1}\,cm^{-1}$ and a ratio $\phi_{fl}^{NBA}/\phi_{fl}^{T} \approx 1/30$ we estimate the fluorescence lifetime τ_{fl} of *o*-NBA to be ∼ 30 fs.

The value of this lifetime is determined by recording the transient fluorescence of *o*-NBA after excitation at 270 nm (Fig. 2). This experiment covers detection wavelengths greater than 385 nm. For smaller wavelengths, the signal is hidden underneath strayed third harmonic light of the gate pulse, which is generated in the Kerr-medium. The emission of *o*-NBA drops below the detection limit within less than a picosecond and shows only weak spectral dependencies. Inspection of time traces (Fig. 2b) shows that the dominant decay time of the fluorescence is of the order of the instrumental response time (∼ 110 fs). But another very weak contribution is also observed which decays within several hundreds of femtoseconds. In the contour representation of the data this contribution is hardly discernible from the noise. For better perception, two ranges of the signal around 400 and 500 nm, respectively, were averaged and normalized with respect to each other (Fig. 2b). Only the time

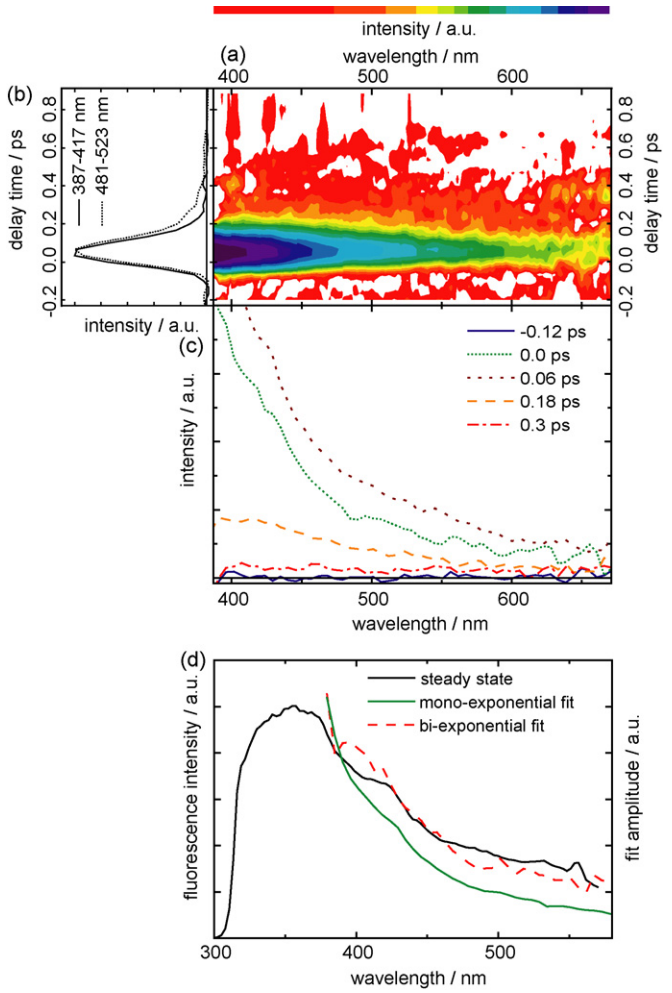

Fig. 2. Femtosecond fluorescence of *o*-NBA after 270 nm excitation. (a) Contour plot of the transient fluorescence. (b) Time traces of the signal averaged between 387–417 nm (solid line) and 481–523 nm (dotted line). (c) Transient fluorescence spectra recorded at delay times as indicated. (d) Steady state fluorescence (black line) compared to the amplitude spectrum of the mono-exponential analysis (60 fs time constant, green line) and the sum of the 50 and 400 fs fit components weighted with the respective decay time, which were obtained from a bi-exponential analysis (green line) (For interpretation of the references to colour in this figure legend, the reader is referred to the web version of the article.).

trace centered around 500 nm features a remarkable amount of this longer lived component. To obtain quantitative information, we have analyzed the data using the global fit procedure as described above. Modeling the data with a single exponential decay yields a time constant of 60 fs. But this analysis fails to properly describe the weak longer lived contribution to the signal at longer wavelengths. A much better agreement between fit and experimental data especially in this spectral region is found using two exponential decay functions with time constants of $\tau_1 = 50$ fs and $\tau_2 = 400$ fs. The value of τ_1 matches the above prediction based on the fluorescence quantum yield. The ratio of the amplitudes of both components can only be estimated as the maximum of the 50 fs contribution is not spectrally resolved and the 400 fs contribution is too weak to extract a proper amplitude spectrum. Yet, in the spectral range accessible the amplitudes of both components differ by roughly two orders of magnitude. Fig. 3 b illustrates the necessity of a bi-exponential modeling of the data: the fluorescence signal averaged between 481 and 523 nm is depicted together with the results of mono- and bi-exponential fits of this data with the time constants of the respective global analysis set as a fixed parameter.

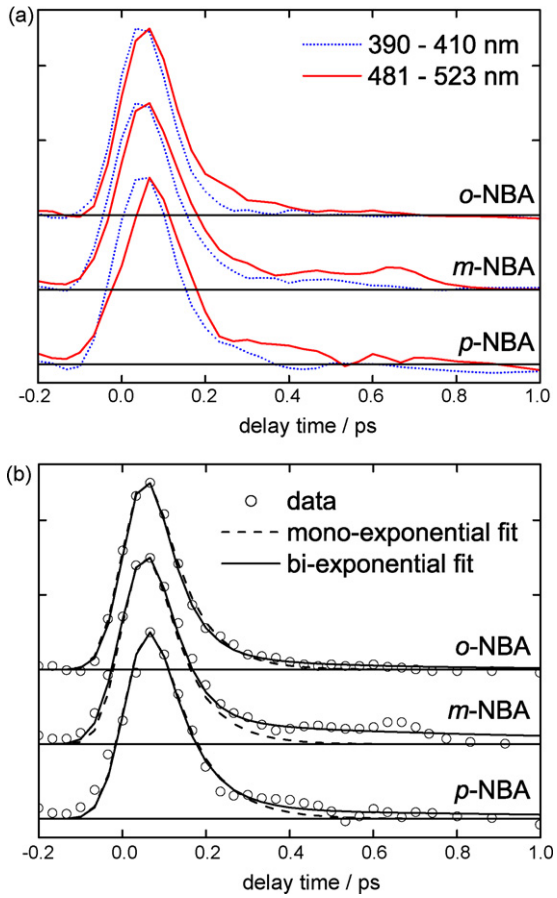

Fig. 3. (a) Normalized time traces of the fluorescence decays of *o*-, *m*-, and *p*-NBA after 270 nm excitation. The signal averaged between 387–417 nm (391–413 nm in case of *p*-NBA) is represented in dotted blue lines and the signal between 480 and 523 nm in red solid lines, respectively. (b) Long wavelength emission decays as in (a) plotted as circles and compared to mono- (dashed lines) and bi-exponential fits (solid lines) of the data with the time constants obtained from the respective global analysis (For interpretation of the references to colour in this figure legend, the reader is referred to the web version of the article.).

Only the bi-exponential analysis properly describes the weak, yet non-negligible signal contributions at later delay times. Another cross-check is possible to substantiate the need of the 400 fs decay component and further to exclude the involvement of any longer lived components. Taken a sum of exponential decays, the time-integrated (steady state) signal $S_{\mathrm{int}}(\lambda)$ is given by the sum of the amplitude spectra $A_i(\lambda)$ weighted with the respective decay time τ_i:

$$S_{\mathrm{int}}(\lambda) = \sum_{i=1}^{n} A_i(\lambda)\tau_i$$

As can be seen from Fig. 2 d, a satisfactory agreement between the static spectrum and the quantity $S_{\mathrm{int}}(\lambda)$ – especially in the red wing of the emission – is only obtained from the bi-exponential analysis which yielded the 50 and 400 fs time constants.

For comparison, the same experiments were conducted for *m*-NBA and *p*-NBA (Fig. 3). Surprisingly, the emission decay patterns of the non-reactive isomers *m*- and *p*-NBA strongly resemble the one of the photo-reactive *o*-NBA: The largest part of the emission signal decays within approximately 200 fs after excitation. As in the case of *o*-NBA, we also observe extremely weak longer lived components for the other isomers. Besides, the amplitudes of these components again seem to be more pronounced at longer wavelengths. For better perception, we have presented two normalized time traces for each isomer—one in the blue and one in the red wing of the detected signal. To enhance the depiction of the longer lived components, we have averaged the signal over several wavelengths—namely between 387 and 417 nm (391–413 nm in case of *p*-NBA) in the blue and between 481 and 523 nm in the red part of the spectrum (Fig. 3a). The data of *m*-NBA and *p*-NBA have been subject to global analyses using single and double exponential decays, respectively. Time constants of 80 fs for *m*-NBA and 90 fs for *p*-NBA were retrieved from the single exponential fits. The bi-exponential modeling of the data yielded decay constants of $\tau_1 = 60$ fs and $\tau_2 = 900$ fs in the case of *m*-NBA as well as $\tau_1 = 80$ fs and $\tau_2 = 1$ ps for *p*-NBA. Here, it has to be stressed that the numerical values of the longer time constants are subject to large errors of up to 95%. Nevertheless, the match between experimental data and fit especially in the red wing of the respective emission is considerably better if a second decay component is included. As in the above-mentioned case of *o*-NBA, this improvement is illustrated by comparing the mono- and bi-exponential analyses of the emission decays of *m*-NBA and *p*-NBA in this spectral region (Fig. 3b). It can be clearly seen that both for *m*-NBA and *p*-NBA the weak longer lived signal contributions cannot be reproduced if only a single exponential decay is taken into account.

3.2. Transient absorption experiments

The absorption changes of all three NBA isomers were recorded after excitation with 258 nm pulses. An inspection of the absorption changes along the time axis exhibits that this excitation induces multi-exponential dynamics in all three cases which take place on several timescales (Fig. 4 a, d and g). For *o*-NBA, we find a broad and structureless induced absorption immediately after excitation (Fig. 4b).[1] The signal afterwards decays and gives way to an absorption band centered around 450 nm (see also Fig. 5). In accordance with the results from matrix isolation spectroscopy [30] and previous results from our group [20] this absorption band can unambiguously be assigned to the first ground state intermediate of the photo reaction of *o*-NBA which is a ketene (Scheme 1). It can be seen that the ketene absorption is already present after several picoseconds but is subject to further slower dynamics. It rises to its maximal signal on the 100 ps timescale and starts to decay in the nanosecond time regime. This decay is strongly dependent on the amount of water in the solvent and takes place on the 10 ns timescale if only traces of water are present. The described kinetics was parametrized using the global fitting routine described in Section 2. To improve the stability of this fit, the global analysis was confined to a maximum delay time of 1 ns where the ketene absorption reaches its maximum value. In plots of decay traces on a logarithmic time axis (see Fig. 4 a), four turning points can be discerned in this time range. Such turning points mark kinetic components. In line with that a singular value decomposition [31] affords four dominant singular values. Therefore, in the global analysis four time constants were used. A good agreement between data and fit was obtained with values for these time constants of $\tau_2 = 0.4$ ps, $\tau_3 = 1.4$ ps, $\tau_4 = 6.6$ ps, $\tau_5 = 220$ ps, and an offset plus the respective decay-associated spectra (Fig. 4c).[2] The time constant $\tau_5 = 220$ ps describes the delayed rise of the ketene

[1] In comparison with our previous results on *o*-NBA in ethanol [20], we observe spectral differences especially at the very blue and red edges of the probed spectrum. We found that these deviations are caused by a chromatic error of the previous setup which has been eliminated in the experiments presented here.

[2] Please note that τ_1 is left out intentionally while numbering the time constants—see Section 4.

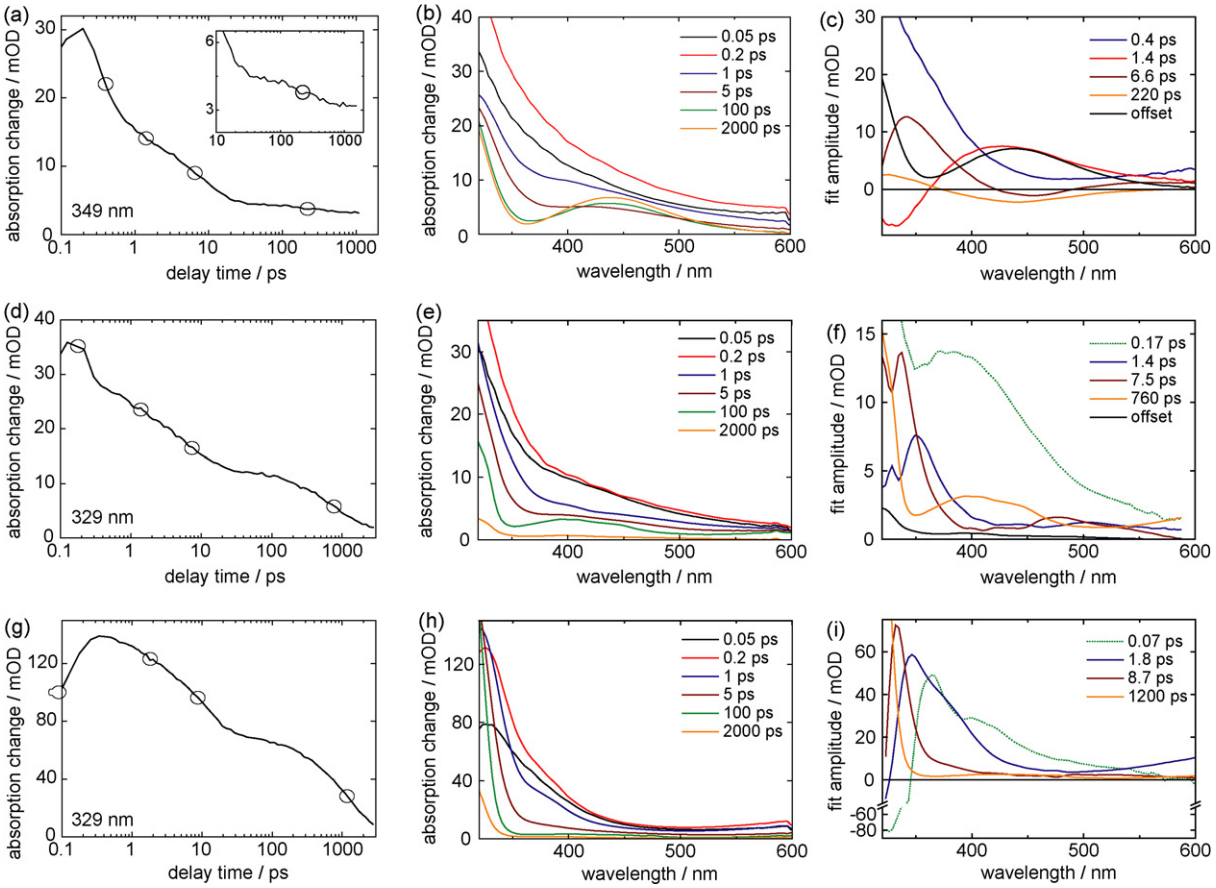

Fig. 4. Transient absorption of *o*-NBA (upper panel), *m*-NBA (center), and *p*-NBA (lower panel) after 258 nm excitation. Time traces of the signal are shown in graphs (a) (at 349 nm), (d and g) (329 nm) on a logarithmic time axis. The circles mark the time constants obtained from the global analysis procedures. The inset in (a) is for a better display of the 220 ps process. Graphs (b), (e), and (h) depict transient spectra taken at delay times as indicated. Graphs (c), (f), and (i) show the decay-associated spectra of the time constants yielded by the global analyses. Please note the axis break and the compression in graph (i) for better perception of the smaller amplitudes. The shortest time constants for *m*- and *p*-NBA and the corresponding amplitude spectra (plotted as dotted lines) are subject to considerable uncertainties.

absorption as indicated by a negative fit amplitude around 450 nm. The decay-associated spectra of the time constants τ_3 and τ_4 (1.4 ps, 6.6 ps) both feature sigmoidal amplitude spectra and together describe an overall blue-shift of the early absorption spectra. The amplitude spectrum associated with the 0.4 ps process shows only positive fit amplitudes and strongly rises towards the UV spectral range. The pronounced dip in this spectrum between 400 and 500 nm indicates that this process can be related to the ketene formation. In the time trace of the transient absorption signal at a probe wavelength of 349 nm the time constants obtained in that manner are marked as circles (Fig. 4a).

Similar to *o*-NBA, the transient absorption of *m*-NBA also shows a broad induced absorption band after excitation (Fig. 4e). The signal decays on the picosecond timescale to form a species which features a distinct absorption band centered around 400 nm and another band whose maximum is not observed as it lies beyond 600 nm, the largest wavelength covered here. The spectrum of this species is most pronounced after several hundreds of picoseconds (see Fig. 5) and subsequently decays on the nanosecond timescale leaving only a weak offset at the largest delay time covered (2 ns). The decay of the transient signal at a probe wavelength of 329 nm exhibits four turning points, indicating that four kinetic processes occur. Consequently, we used four exponential decay components to model the data in the corresponding global analysis. The respective decay-associated spectra as well as the weak remaining offset are shown in Fig. 4 f: The time constant $\tau_1 = 0.17$ ps obtained by this analysis describes the decay of the initially observed broad induced absorption. As its value is close to the width of the instrumental response function and further the data around time zero is not perfectly described by this fit, this time constant and the shape of the respective spectrum are subject to uncertainties. The subsequent processes feature characteristic time constants of $\tau_2 = 1.4$ ps and $\tau_3 = 7.5$ ps followed by the decay of the species with the absorption bands around 400 nm and in the very red wing of the covered

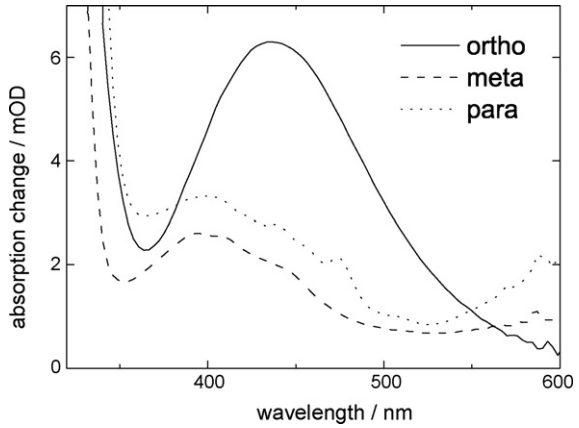

Fig. 5. Transient absorption spectra of *o*- (solid line), *m*- (dashed), and *p*-NBA (dotted) taken 250 ps after excitation at 258 nm. On this timescale the different outcome of the photo excitation of *o*-NBA as compared to *m*- and *p*-NBA is most pronounced.

Table 1
Compilation of the time constants in picoseconds and their estimated errors determined is this study for the three NBA isomers by ultrafast emission and absorption experiments

	o-NBA	*m*-NBA	*p*-NBA	Error (%)
Emission				
τ_1	0.05	0.06	0.08	±15
τ_2	0.4	0.9	1.0	+95, −45
Transient absorption				
τ_1	–	0.17	0.07	±25
τ_2	0.4	1.4	1.8	+50, −25
τ_3	1.4	7.5	8.7	+30, −15
τ_4	6.6	–	–	+65, −35
τ_5	220	760	1200	±15

spectral range with $\tau_5 = 760$ ps.[3] In the visible spectral range, the spectra associated with τ_2 and τ_3 together roughly exhibit a mirror symmetry to the spectrum of τ_5 indicating that the species decaying within 760 ps is at least partially formed by these processes.

The transient spectra taken after excitation of *p*-NBA (Fig. 4h) strongly resemble the ones of *m*-NBA. Differences to our observations on *m*-NBA are that the initially appearing broad absorption shows stronger contributions in the red wing of the spectrum and that a delayed rise of the signal is observed in the UV spectral range. The latter feature is clearly seen by comparing the time traces of the transient absorption of both isomers at 329 nm (Fig. 4 d and g). Further, the overall signal magnitudes for delay times <10 ps are much larger in the case of *p*-NBA. At later delay times, a species featuring absorptions around 400 nm and beyond 600 nm can also be identified (Fig. 5). It features a signal amplitude of ∼ 5 mOD which is similar to the corresponding signal of *m*-NBA. Thus, as both experiments have been carried out under identical conditions the absorption strengths of the corresponding species are of similar magnitude. Again, this species decays within ∼ 1 ns to leave only a small offset absorption at the latest delay times covered with our setup. The time trace of the signal at 329 nm depicted in Fig. 4 g indicates that multiple processes on several timescales occur. The global analysis well reproduces the data using four time constants. It yields values of $\tau_1 = 0.07$ ps, $\tau_2 = 1.4$ ps, $\tau_3 = 8.7$ ps, and $\tau_5 = 1200$ ps[4] as well as an offset and the respective decay-associated spectra (Fig. 4i). The process proceeding with τ_5 is again linked to the decay of the species with the absorption bands around 400 nm and beyond 600 nm. The spectrum associated with τ_3 features only positive amplitudes and resembles the one of τ_3 found for *m*-NBA. The process described by τ_2 marks the decay of the initially observed induced absorption as the associated spectrum is very similar to the transient spectrum recorded after 0.2 ps (Fig. 4h). The shortest time constant τ_1 represents a very fast contribution to the decay of this absorption but features a negative fit amplitude in the very blue part of the spectrum. It thus describes the delayed rise of the signal observed there which is best seen in Fig. 4 g.

For better comprehension Table 1 summarizes the time constants derived from the emission and absorption experiments of all three NBA isomers.

4. Discussion

We have measured the ultrafast dynamics of all three NBA isomers by means of fluorescence and absorption spectroscopy. The fluorescence dynamics of all three samples are found to be strikingly similar: The largest part of the fluorescence signal decays within $\tau_1 < 100$ fs. In addition, very weak contributions to the signal with lifetimes τ_2 of ∼0.4–1.5 ps are found in the red wing of the transient fluorescence. The pronounced red wings can be taken as an indication for structural distorsions in the excited state and/or the contribution of more than one excited state to the fluorescence emission. One would expect that the two time constants seen in the fluorescence data are also measured in the transient absorption experiment. Allowing for rather large errors this turns out to be true for *m*- and *p*-NBA. For *o*-NBA similar values for $\tau_2 \sim 400$ fs are found in both experiments but the shortest time constant $\tau_1 = 50$ fs of the emission decay cannot be retrieved from the absorption data. This could be due to the fact that – judged from the fluorescence experiment – in this case the two time constants are closer to each other. Further, they are close to the instrumental response time of the absorption experiment (∼ 200 fs). Both facts might explain why the fitting procedure fails to disentangle these two processes, here. Still, based on the fluorescence data one can unequivocally state that all isomers feature a sub 100 fs decay process which goes along with a strong decrease of oscillator strength. For *p*-NBA – the compound with the strongest ground state absorption – this process even shows up in the transient absorption experiment as a decaying stimulated emission. In all three cases, this initial dynamic is followed by a ∼ 1 ps process observed in both experiments as a decay of a weak fluorescence component and the decay of an induced absorption band, respectively.

A possible interpretation of the early dynamics associated with τ_1 and τ_2 could be based upon the results by Peon and co-workers who investigated nitrated polyaromatics by means of fluorescence up-conversion and also observed bi-exponential emission decays with fast time constants in the 100 fs range and slow contributions on the picosecond timescale [9]. They have assigned the fast components to a structural change within the initially excited singlet state, whereas the slower decays were associated with intersystem crossing to the triplet manifold. The structural change on the 100 fs timescale could for instance be related to a twist of the nitro group out of the aromatic plane as observed in related nitrated aromatic molecules (*p*-nitroanilines) [32,33]. If this model held in the case of NBA, the process associated with τ_1 would be related to a relaxation within the initially excited state with a concomitant loss of oscillator strength, e.g. a twist of the nitro group. The subsequent decay of the relaxed state would then proceed with the time constant τ_2.

Still, some important differences to the study on the polycyclic nitrated aromatics have to be pointed out. Contrary to the work performed by Peon and co-workers we do not excite the NBA isomers to the lowest lying excited state as easily seen by inspection of the UV–vis spectrum of *o*-NBA (Fig. 1). In a very recent joint theoretical and experimental approach relying on state of the art multi-reference ab initio methods, we aim at the assignment of the bands observed in this spectrum [26]. There it is shown that the state initially excited in our experiments is most likely a $\pi\pi^*$ state with charge transfer character. In accordance with the experimental spectrum, these calculations further predict the existence of several lower lying excited states which are of $n\pi^*$ character and feature only weak oscillator strengths. Similar observations have been made for the closely related nitrobenzene [34,35] whose absorption spectrum strongly resembles the one of the NBA isomers [36]. This is in contrast to the situation prevailing in the molecules investigated by Peon and co-workers, where the lowest lying excited singlet state is believed to be of $\pi\pi^*$ nature [9,10]. Consequently, these nitrated polycyclic aromatics lack a relaxation channel to lower excited states which is accessible for the NBA isomers investigated here.

An alternative explanation for our findings will be outlined now. Obviously, the initial dynamics associated with the time constants

[3] Please note that τ_4 is left out intentionally while numbering the time constants—see Section 4.
[4] Please note that τ_4 is left out intentionally while numbering the time constants—see Section 4.

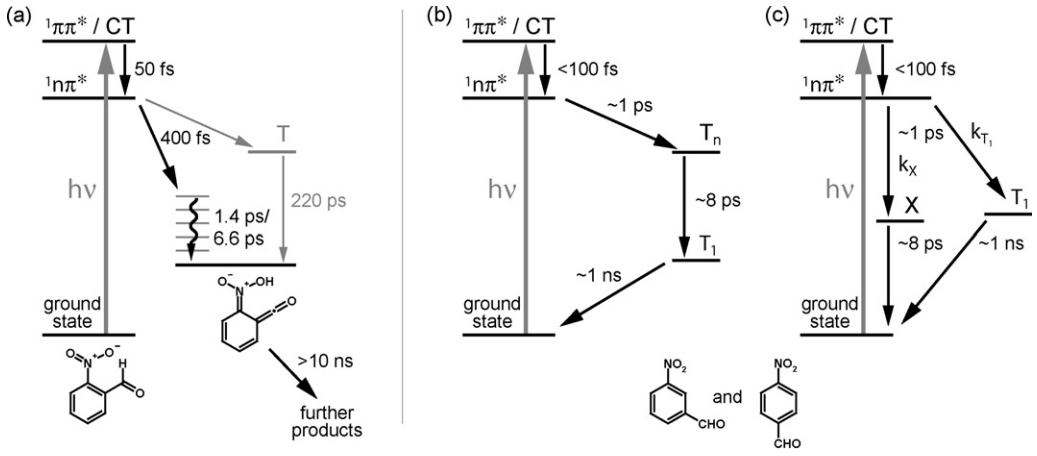

Scheme 2. Schematics depicting the excited states and processes occurring after photo-excitation of the NBA isomers. (a) Model for *o*-NBA. In the cases of *m*- and *p*-NBA either a sequential (b) or a branched scheme (c) is conceivable. The time constants derived in this study are assigned to the respective dynamics.

τ_1 and τ_2 are independent of the position of the aldehyde moiety on the aromatic ring. Again referring to the theoretical assignments of the electronically excited states of *o*-NBA [26] and the parent molecule nitrobenzene [34,35] these early processes can be assigned as follows (see also Scheme 2): by exciting the NBA isomers at 270 nm a bright charge transfer state is populated. Transition to one of the energetically lower lying $n\pi^*$ states takes place within $\tau_1 < 100$ fs. This transformation goes along with a large loss of oscillator strength and a red-shift of the emission (Fig. 3). Consequently, the subsequent decay of this state features an emission signal which is by orders of magnitude lower than that of the initial signal. The τ_2 time constants would then be associated with the decay of this successor state. In the case of *o*-NBA, it is this successor state from which the ketene is formed as inferred from the transient absorption experiment. Thus, we can relate an excited state decay to the photochemistry of *o*-NBA. In addition, we have found a relaxation process prepending the ketene formation. Interestingly, the relaxation pattern within the singlet manifold is basically the same also for the non-reactive NBA isomers.

To assign the signatures and dynamics which are exclusively observed in the transient absorption experiments (τ_{3-5}) one best starts with the slow processes as these can be linked to previous results. Upon irradiation of *o*-NBA, *o*-nitrosobenzoic acid is formed with a quantum yield of ~ 50% via a ketene intermediate. As mentioned above, the visible absorption band peaking at 450 nm observed at late delay times can clearly be assigned to this ketene intermediate in the electronic ground state by comparison with previous results [20,30]. The lifetime of this ketene in acetonitrile has been reported to be around 20 ns [18,19] which cannot be covered with our femtosecond setup. We estimate the decay of this species to take place within ~ 10 ns which is of the same timescale. An acceleration of the decay of the ketene in our experiment (as compared to the literature values) can be attributed to traces of water in the solvent or in the sample circuit used in our experiments. The time constant $\tau_5 = 220$ ps features a negative amplitude at the wavelengths of the ketene absorption which indicates that a portion of the ketene is formed with this time constant. By comparing the amplitude of the spectrum related to τ_5 with the offset spectrum at 450 nm, one can estimate that the fraction of the ketene formed via this channel amounts to ~ 1/3. Although, the largest fraction of the ketene is already formed after < 10 ps (Fig. 4b), this finding might indicate the participation of a "slow" pathway to the ketene formation—probably via a triplet state. This possibility is discussed in detail in another publication [37]. Still, the process associated with $\tau_3 = 1.4$ ps and $\tau_4 = 6.6$ ps in the case of *o*-NBA have to be understood. The ketene is formed in its electronic ground state with a considerable amount of vibrational excess energy and thus cooling processes are expected. For *o*-NBA in ethanol vibrational cooling of the nascent ketene has been directly observed by ultrafast infrared spectroscopy [20] to take place on the timescale of some picoseconds. While analyzing the data presented here, we could not obtain a satisfactory agreement between fit and data using only a single time constant to model this process which reflects the non-exponentiality of cooling dynamics. Much better results were achieved by including another time constant into the fitting procedure. We thus attribute the time constants τ_3 and τ_4 to vibrational cooling of vibrationally hot ground state species (Scheme 2). The sigmoidal shape of the respective amplitude spectra as well as the values of τ_3 and τ_4 match the ones observed for vibrational cooling of a comparable molecular probe in acetonitrile [33,38].

The commonalities we have observed for the early dynamics of the three NBA isomers are in strong contrast to the obvious differences in the slower processes between *o*-NBA and its non-reactive isomers. For *m*- and *p*-NBA several picoseconds after excitation a species with an absorption band around 400 nm and another one extending beyond 600 nm is observed (Fig. 5). It decays within approximately 1 ns (Fig. 4 d–i). Almost identical spectral signatures have been observed in transient absorption experiments by Yip et al. for nitrobenzene and the closely related *o*- and *p*-nitrotoluene [12]. These absorptions had lifetimes of ~ 700 ps and were assigned to an $n\pi^*$ triplet state. This assignment has later been confirmed by Takezaki et al. in transient grating experiments on the same molecules [13]. They have further reported very similar triplet lifetimes and triplet quantum yields of about 0.8. According to these results, we assign the $\tau_5 \sim 1$ ns decay time constants and the respective spectral signatures of *m*- and *p*-NBA to a triplet state (T_1 in Scheme 2 b and c). Especially in the visible spectral range, the spectra of the τ_3 time constants roughly exhibit a mirror symmetry to these triplet decay spectra indicating that the τ_3 process populates this triplet state. Assuming that the excited singlet states are depopulated within roughly one picosecond as inferred from the fluorescence experiments, the τ_3 process is likely to take place in the triplet manifold. In a transient grating study on nitrobenzene, Takezaki et al. have observed a 6 ps time constant and assigned it to a triplet–triplet internal conversion [39]. Such a process would be in line with our findings. The triplet state lowest in energy (T_1) would then be populated from a triplet state higher in energy which is denoted as T_n in Scheme 2 b. It should be stressed that the value of $\tau_3 \approx 8$ ps is not in conflict with the assignment to a decay of a higher

triplet state. Recent measurements of triplet internal conversions in aromatic carbonyl compounds yielded even longer time constants [40,41]. If such a sequential model holds the similarity of the time constants $\tau_4 = 6.6$ ps in the case *o*-NBA with the values of τ_3 of the non-reactive isomers would be purely coincidentally. Still, another model is conceivable to hold responsible for the observed kinetics: In a branched reaction scheme the time constant τ_2 could describe the parallel build-up of the triplet state T_1 and of another spectroscopic state (denoted X in Scheme 2c) which afterwards decays with the time constant τ_3. A distinction between a sequential and a branched kinetic scheme can be based on inspection of the actual spectra of the spectroscopic states involved—not to be confused with the transient difference spectra and the amplitude spectra derived from the global analysis. Under certain assumptions, these spectra can be obtained by using the eigenvectors of the rate matrix of the proposed model for each eigenvalue as described in, e.g. ref. [42,43]. We have carried out such an analysis under the assumption of different branching ratios. Spectra with reasonable absorption cross-sections for T_1 and X were only obtained if the population was distributed with comparable rates k_{T_1} and k_X among these states. A branching with a ratio of k_{T_1}/k_X of, e.g. 1/10 or vice versa afforded spectra with unrealistically high absorption cross-sections. We conclude that based on the present findings, we cannot finally discern between a sequential and a branched kinetic scheme for *m*- and *p*-NBA. Still, the triplet quantum yields of *p*-NBA [44] as well as the one of the related nitrobenzene [13] are assumed to be close to unity. These findings as well as the conclusions drawn by Takezaki et al. in the case of nitrobenzene [39] render the sequential model more likely.

5. Conclusion

We have conducted a comprehensive investigation on the ultrafast dynamics of a photo-reactive and two non-reactive derivatives of nitrobenzene, namely *o*-, *m*-, and *p*-NBA. To the best knowledge of the authors, we thereby present the first time-resolved emission data on nitrobenzene derivatives. To sum up our results on the three isomers of NBA, we will use Scheme 2 as a guidance. Surprisingly, we found that the fluorescence dynamics of all three molecules are almost identical and exhibit a bi-phasic decay with time constants of $\tau_1 < 100$ fs and $\tau_2 \sim 1$ ps. We assign these processes to a transition of the initially excited electronic state which is most likely of $^1\pi\pi^*$ nature to a $^1n\pi^*$ state and the depletion of the latter state, respectively. The subsequent dynamics – probed by transient absorption spectroscopy – exhibit striking differences between *o*-NBA and its non-reactive isomers in the eventual outcome of the photo excitation. For *o*-NBA the decay of the $^1n\pi^*$ state goes along with the formation of a ketene in the electronic ground state, which experiences vibrational cooling dynamics and subsequently decays on the 10 ns timescale. A considerable fraction of the ketene is formed in a much slower process (220 ps)—possibly via a triplet state. For the non-reactive isomers *m*- and *p*-NBA, the decay of the $^1n\pi^*$ state yields a species which decays on the 10 ps timescale to form a triplet state which is identified by its distinct absorption bands around 400 nm and beyond 600 nm. This triplet state decays within ~ 1 ns. We assume that the preceding 10 ps process also takes place within the triplet manifold and thus describes the decay of an initially populated triplet state T_n. Still, at present a branched reaction scheme as depicted in Scheme 2 c cannot be ruled out to hold for *m*- and *p*-NBA.

Acknowledgements

This work was supported by the "Deutsche Forschungsgemeinschaft" through project GI349/1-2 and the DFG-Cluster of Excellence Munich-Centre for Advanced Photonics. The authors are very grateful to W. Zinth for continuous support and fruitful discussions. B.H. acknowledges a scholarship donated by the "Fonds der Chemischen Industrie".

References

[1] H.G. Franck, J.W. Stadelhofer, Industrial Aromatic Chemistry: Raw Materials – Processes – Products, Springer–Verlag, 1988.
[2] C.G. Bochet, J. Chem. Soc., Perkin Trans. 1 (2002) 125.
[3] A.P. Pelliccioli, J. Wirz, Photochem. Photobiol. Sci. 1 (2002) 441.
[4] D. Wöll, J. Smirnova, W. Pfleiderer, U.E. Steiner, Angew. Chem. Int. Ed. 45 (2006) 2975.
[5] T.W. Greene, P.G.M. Wuts, Greene's Protective Groups in Organic Synthesis, John Wiley & Sons, 2007.
[6] X.L. Gao, E. Gulari, X.C. Zhou, Biopolymers 73 (2004) 579.
[7] G. Mayer, A. Heckel, Angew. Chem. Int. Ed. 45 (2006) 4900.
[8] G.C.R. Ellis-Davies, Nat. Methods 4 (2007) 619.
[9] R. Morales-Cueto, M. Esquivelzeta-Rabell, J. Saucedo-Zugazagoitia, J. Peon, J. Phys. Chem. A 111 (2007) 552.
[10] J.S. Zugazagoitia, C.X. Almora-Diaz, J. Peon, J. Phys. Chem. A 112 (2008) 358.
[11] R. Hurley, A.C. Testa, J. Am. Chem. Soc. 90 (1968) 1949.
[12] R.W. Yip, D.K. Sharma, R. Giasson, D. Gravel, J. Phys. Chem. 88 (1984) 5770.
[13] M. Takezaki, N. Hirota, M. Terazima, J. Phys. Chem. A 101 (1997) 3443.
[14] O.F. Mohammed, E. Vauthey, J. Phys. Chem. A 112 (2008) 3823.
[15] G. Ciamician, P. Silber, Chem. Ber. 35 (1901) 2040.
[16] E. Bamberger, F. Elger, Justus Liebigs Annalen Der Chemie 475 (1929) 288.
[17] G.G. Wubbels, T.F. Kalhorn, D.E. Johnson, D. Campbell, J. Org. Chem. 47 (1982) 4664.
[18] M.V. George, J.C. Scaiano, J. Phys. Chem. 84 (1980) 492.
[19] R.W. Yip, D.K. Sharma, Res. Chem. Intermed. 11 (1989) 109.
[20] S. Laimgruber, W.J. Schreier, T. Schrader, F. Koller, W. Zinth, P. Gilch, Angew. Chem. Int. Ed. 44 (2005) 7901.
[21] P.D. Mayo, S.T. Reid, Q. Rev. 15 (1961) 393.
[22] B. Schmidt, S. Laimgruber, W. Zinth, P. Gilch, Appl. Phys. B 76 (2003) 809.
[23] I.B. Berlman, Handbook of Fluorescence Spectra of Aromatic Molecules, second ed., Academic Press, 1971.
[24] S. Laimgruber, H. Schachenmayr, B. Schmidt, W. Zinth, P. Gilch, Appl. Phys. B 85 (2006) 557.
[25] M.J. Tauber, R.A. Mathies, X.Y. Chen, S.E. Bradforth, Rev. Sci. Instrum. 74 (2003) 4958.
[26] V. Leyva, I. Corral, T. Schmierer, B. Heinz, F. Feixas, A. Migani, L. Blancafort, P. Gilch, L. Gonzalez, J. Phys. Chem. A 112 (2008) 5046.
[27] P.R. Callis, Ann. Rev. Phys. Chem. 34 (1983) 329.
[28] D. Onidas, D. Markovitsi, S. Marguet, A. Sharonov, T. Gustavsson, J. Phys. Chem. B 106 (2002) 11367.
[29] J.B. Birks, Photophysics of Aromatic Molecules, Wiley-Interscience, 1970.
[30] S. Kuberski, J. Gebicki, J. Mol. Struct. 275 (1992) 105.
[31] H. Satzger, W. Zinth, Chem. Phys. 295 (2003) 287.
[32] S.A. Kovalenko, R. Schanz, V.M. Farztdinov, H. Hennig, N.P. Ernsting, Chem. Phys. Lett. 323 (2000) 312.
[33] S.A. Kovalenko, S. Schanz, H. Hennig, N.P. Ernsting, J. Chem. Phys. 115 (2001) 3256.
[34] M. Takezaki, N. Hirota, M. Terazima, H. Sato, T. Nakajima, S. Kato, J. Phys. Chem. A 101 (1997) 5190.
[35] O. Kröhl, K. Malsch, P. Swiderek, Phys. Chem. Chem. Phys. 2 (2000) 947.
[36] S. Nagakura, M. Kojima, Y. Maruyama, J. Mol. Spectrosc. 13 (1964) 174.
[37] S. Laimgruber, T. Schmierer, P. Gilch, K. Kiewisch, J. Neugebauer, Phys. Chem. Chem. Phys. 10 (2008) 3872.
[38] Y. Kimura, M. Fukuda, O. Kajimoto, M. Terazima, J. Chem. Phys. 125 (2006) 194516.
[39] M. Takezaki, N. Hirota, T. Terazima, J. Chem. Phys. 108 (1998) 4685.
[40] B. Heinz, B. Schmidt, C. Root, H. Satzger, F. Milota, B. Fierz, T. Kiefhaber, W. Zinth, P. Gilch, Phys. Chem. Chem. Phys. 8 (2006) 3432.
[41] D. Wöll, S. Laimgruber, M. Galetskaya, J. Smirnova, W. Pfleiderer, B. Heinz, P. Gilch, U.E. Steiner, J. Am. Chem. Soc. 129 (2007) 12148.
[42] W. Holzapfel, U. Finkele, W. Kaiser, D. Oesterhelt, H. Scheer, H.U. Stilz, W. Zinth, Proc. Natl. Acad. Sci. U.S.A. 87 (1990) 5168.
[43] T. Cordes, B. Heinz, N. Regner, C. Hoppmann, T.E. Schrader, W. Summerer, K. Rück-Braun, W. Zinth, ChemPhysChem 8 (2007) 1713.
[44] H. Görner, H.J. Kuhn, J. Phys. Chem. 90 (1986) 5946.